Efficient Treatment of Lead-containing Wastewater Using Bagasse Biochar Modified *via* Hydroxylapatite

Qing Zhang, Lin Lu, Meina Liang,* Dunqiu Wang, Daolin Huang, and Yinian Zhu

A hydroxylapatite bagasse biochar composite was prepared *via* the hydrothermal chemical precipitation method with bagasse as the primary raw material. The adsorption capacity of hydroxylapatite bagasse biochar composite for Pb(II) was determined using a series of batch adsorption experiments. The results showed that the point of zero charge value was near neutral pH, and the optimal pH ranged from 4.0 to 7.0. Langmuir isotherms were suitable for fitting the isothermal adsorption process of Pb(II) by the hydroxylapatite bagasse biochar composite. The maximum adsorption capacity of hydroxylapatite bagasse biochar composite in terms of Pb(II) was 210 $mg \cdot g^{-1}$ at 25 °C. Fourier transform infrared spectrometry analysis indicated that oxygen-containing functional groups were abundant on the external and internal surfaces of the composite sample, which provided numerous chemical sorption sites and resulted in an increase in the adsorption capacity of the composite sample. The Pb(II) removal mechanism of the hydroxylapatite bagasse biochar composite primarily utilized surface diffusion, electrostatic attraction, surface complexation, ion exchange, and a dissolving-coprecipitation reaction. The composite sample was suitable for the treatment of lead-contaminated water (containing zinc, arsenic, cadmium, *etc.*), which was a promising environmentally friendly material.

DOI: 10.15376/biores.17.1.1205-1231

Keywords: Hydroxylapatite; Bagasse biochar; Lead; Adsorption

*Contact information: School of Environmental Science and Engineering, Guilin University of Technology, Guilin 541004 P.R. China; *Corresponding author: liangmeinaa@163.com*

INTRODUCTION

Many industrial activities and manufacturing products, *e.g.*, batteries, alloys, pigments, paints, smelting, mining, ceramics, and power generation, result in the introduction of Pb(II) to the environment (Meski *et al.* 2010). Pb(II) causes kidney and brain damage, a loss of learning ability in children, increased blood pressure, and a disruption in hemoglobin formation (Argun *et al.* 2007). Conventional lead wastewater treatment methods, *e.g.*, chemical precipitation, ion-exchange, reverse osmosis, and electrochemical treatment, can produce large amounts of chemical sludge, which may pollute the environment in further treatment (Elouear *et al.* 2008). Hence, there was a need for economical, less toxic, renewable, sustainable, and easily operated techniques for the removal of heavy metal ions from wastewater (Crini 2005). Adsorption is an effective, energy-saving, and easily operated method for removing trace concentrations of contaminants, including heavy metals, from water. Its application to agricultural and industrial residues for the removal of heavy metals from water has been a focus of research in recent decades (Chand and Pakade 2015; Liang *et al.* 2018).

The chemical formula of hydroxyapatite (HAP) is $Ca_{10}(PO_4)_6(OH)_2$, the most stable calcium hydrogen phosphate compound with pH from 4 to 12, and the mole ratio of calcium to phosphorus is 1.67. This crystal chemical characteristic enables different types of heavy metals to replace the position of calcium in hydroxyapatite, so it has good ion adsorption and exchange characteristics. Recently, HAP has attracted considerable interest in the environmental field because of its high removal capacity for various heavy metals, *e.g.*, Pb(II), Cu(II), and Cd(II), from water bodies (Saber-Samandari *et al.* 2014; Yan *et al.* 2014; Jayakodiarachchi and Jayaweera 2015). Hydroxylapatite and its composites have been reported as adsorbents for the removal of Co(II), Ni(II), and Pb(II) as well as organic compounds from aqueous solutions (Gupta *et al.* 2012). In Chand's work, hydroxyapatite nanoparticles were synthesized, and removal of Pb(II), Cd(II), and Ni(II) has been investigated. Langmuir models are fitted equally well the adsorption data for three ions under consideration, maximum adsorption capacity followed the order: Pb(II) >Cd(II) > Ni(II) (Chand and Pakade 2015).

However, hydroxylapatite-based materials have weak mechanical strength. Moreover, the separation of HAP nanoparticles from the treated effluents is cost-prohibitive, time-consuming, and difficult to perform. Subsequently, the current challenges can be solved by coating HAP on to a fibrous network of highly porous bagasse, which produces a system that overcomes the hindrances associated with the physical characters of the nanomaterials, *i.e.*, solid/liquid separation, poor mechanical strength, and small particle size. The annual bagasse production was approximately 200 million tons globally (Satyanarayana *et al.* 2007). Since the primary components of bagasse are cellulose, hemicellulose, and lignins, it was an ideal material for preparing a biomass adsorbent. In addition, hydroxyapatite bagasse biochar (HAP-BC) was used to adsorb As(Ⅴ) in previous work (Yan *et al*. 2019). However, HAP-BC for lead removal has not been reported.

In this study, hydroxylapatite bagasse biochar (HAP-BC), with bagasse as the primary raw material, was prepared and the Pb(II) adsorption characteristics of HAP-BC were studied. The effect of various factors, *e.g*, contact time, pH, Pb(II) concentration, and bagasse content, on the metal adsorption capacity of HAP-BC were studied using a series of batch experiments. The Langmuir adsorption isotherm and surface complex formation model were used to describe the adsorption characteristics of Pb(II) *via* aqueous HAP-BC.

EXPERIMENTAL

Materials

The calcium oxalate, sodium hydroxide, hydrochloric acid, ammonia, and lead nitrate were all analytical grade. The ammonium acetate and ammonium dihydrogen phosphate were all reagent grade. Bagasse, with marrow, was obtained from a sugar industry in Guigang, Guangxi, China.

Preparation of HAP-BC

Preparation of the HAP-BC and SB-BC (sugarcane bagasse biochar) are outlined in the supporting information S1 from the authors' earlier work (Yan *et al*. 2019). Figure 1 shows the preparation flow chart of the HAP-BC.

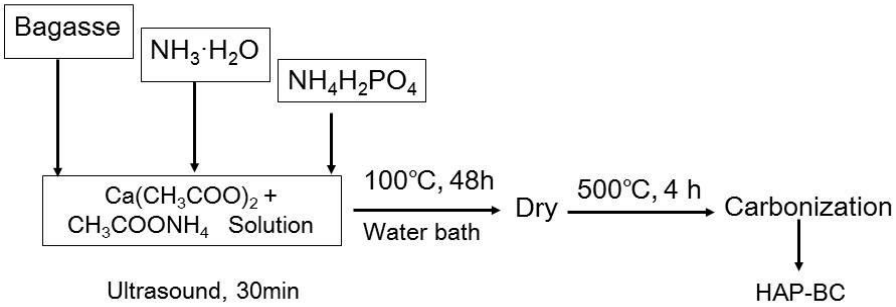

Fig. 1. The preparation flow chart of the HAP-BC

Characterization of HAP-BC

The as-prepared HAP-BC sample was systematically analyzed *via* scanning electron microscopy (SEM) (JSM-6380LV, JEOL Ltd., Tokyo, Japan), energy dispersive X-ray spectroscopy (EDS) (JEM-6380LV, JEOL Ltd., Tokyo, Japan), scanning electron microscopy (TEM, JSM-6380LV, JEOL, Japan), Fourier transform infrared spectroscopy (FT-IR) (CAT500A, PerkinElmer, Waltham, MA), X-ray photoelectron spectroscopy (XPS) (Thermo Fisher Scientific Inc., Waltham, MA), and X-ray diffraction (XRD) (X'Pert PRO X, Malvern Panalytical, Malvern, UK). The specific surface area was determined according to the Brunauer-Emmet-Teller (BET) equation using a Quantachrome Nova Station apparatus (Beijing Jingwei Gaobo Science and Technology Co., Ltd., Beijing, China). The pH was recorded with a pH meter (PHM250). Furthermore, the zeta potential was measured as a function of the pH in a NaCl electrolyte solution with a Malvern Zetasizer Nano ZS90 (Malvern Panalytical Ltd, Malvern, England). The XPS experiments were performed with a ESCALAB 250Xi (Thermo Electron Corporation, Waltham, USA) using an Al Kα X-ray source (1486.6 eV). The residual Pb(II) concentration was determined *via* atomic absorption spectrometry (AAnalyst 700, PerkinElmer, Waltham, MA, USA).

Batch Experiments

The sorption performance of HAP-BC for Pb(II) was evaluated *via* the batch technique under different conditions. First, the desired amounts of HAP-BC powder were weighed and put into 100 mL plastic centrifuge tubes. Then, 50 mL of Pb(II) solution at different concentrations was added, after pH adjustments. The tubes were sealed with capsules and shaken with a temperature shaker (at 25 °C, 35 °C, and 45 °C) at 200 $r \cdot min^{-1}$ overnight, allowing the adsorption to reach equilibrium. After centrifugation with 4000 $r \cdot min^{-1}$ for 5 min, all the samples were filtered through a 0.45 μm micropore membrane and spiked with 0.2 % (V/V) HNO_3 in 100 mL volumetric flasks.

The removal of Pb(II) on HAP-BC was calculated using Eq. 1,

$$Removal(\%) = \frac{C_0 - C_e}{C_0} \times 100\% \quad (1)$$

where C_e ($mg \cdot L^{-1}$) is the final concentration and C_0 ($mg \cdot L^{-1}$) is the initial concentration. The amount of Pb(II) loaded on the HAP-BC sample was determined by Eq. 2,

$$Q_e = \frac{C_0 - C_e}{m} \times V \quad (2)$$

where Q_e (mg·g^{-1}) is the amount of loaded Pb(II), V (L) is the solution volume, and m (mg) is the mass of the HAP-BC.

The following operating parameters that may affect Pb(II) adsorption were studied: the contact time (30 min to 2160 min), the solution pH (2.0 to 9.0), the adsorbent dosage (1.00 g·L^{-1} to 6.00 g·L^{-1}), the initial Pb(II) concentration (10 mg·L^{-1} to 500 mg·L^{-1}), and temperature (25 °C to 45 °C). The adsorption isotherm, the adsorption rate, and the thermodynamic parameters were obtained and analyzed at a pH of 7.0.

Reusability Experiments

Reusability experiments were used to test the stability and reusability of the HAP-BC. The HAP-BC was magnetically separated and re-dispersed into 0.5 mol L^{-1} of a Na_2CO_3 solution for 6 h, after reaching sorption equilibrium. The HAP-BC was used for regeneration experiments; it was washed with 0.1 mol L^{-1} HCl solution and ultra-pure water three times, respectively. Then the regenerated HAP-BC was applied for the next cycle of sorption experiments.

RESULTS AND DISCUSSION

Characteristics of Hydroxylapatite Bagasse Biochar Composite (HAP-BC)

The size and shape of the hydroxylapatite (HAP) particles on the HAP-BC surface are shown in Fig. 2a. The size of the HAP particles ranged from 150 and 300 nm. The XRD characterization of the HAP-BC was in agreement with the HAP reference in terms of both the peak position and relative intensity, which recorded diffraction peaks at 2θ = 25.93°, 31.85°, 39.86°, 46.78°, 49.45°, and 53.45°, which corresponded to the (002), (211), (130), (222), (213), and (004) facets of hydroxylapatite, respectively (Reference code 00-001-1008), confirming the formation of HAP. The diffraction peak at 2θ = 44.54° belonged to carbon (Reference code 00-011-0646), *i.e.*, a carbonization product of sintered bagasse (as shown in Fig. 2b).

The FTIR spectra of the HAP-BC, bagasse biochar, and activated carbon are shown in Fig. 2c. The absorption peaks of the HAP-BC, bagasse biochar, and activated carbon were at 3428, 3413, and 3391 cm^{-1}, 1600, 1577, and 1569 cm^{-1}, and 1379, 1386, and 1379 cm^{-1}, respectively. The -OH functional groups appeared at 3391 to 3428 cm^{-1} and the C=O functional groups appeared at 1569 to 1600 cm^{-1}. The peak at 1379 to 1386 cm^{-1} was the bending vibration of the -COOH and phenolic groups (Xu *et al.* 2008). The absorption peaks at 1036, 601, and 563 cm^{-1} were the symmetrical stretching vibrational peaks of a tetrahedron of PO_4^{3-}, while the spectra of the sugarcane bagasse biochar and activated carbon exhibited no adsorption peaks at the same wavenumber (1036, 601, and 563 cm^{-1}). The FTIR absorption peaks of the HAP-BC were at 1097 and 1036 cm^{-1}, which were characteristic of hydroxylapatite, further confirming the formation of HAP (Corami *et al.* 2008). The oxygen-containing functional groups were abundantly present on the external and internal surfaces of the HAP-BC, as the adsorption sites contributed to the ion adsorption capacity of HAP-BC.

The specific surface area of HAP-BC was 89.52 m^2·g^{-1} (Yan *et al.* 2019), which was determined by the BET N_2 adsorption method. At the same carbonization temperature, the specific surface area of HAP-BC was approximately 6, 10, 2.5, 2, and 10 times that of spruce, white poplar, rice husk, orange peel, and magnetic modified oak biomass carbon, respectively (Kloss *et al.* 2012; Liu *et al.* 2012). The average pore diameter and total pore

volume were 1.25 nm and 29.26 $cm^3 \cdot g^{-1}$, respectively.

The zeta potential as a function of pH is shown in Fig. S1, the pH_{zpc} was 7.1 and 4.40 for HAP-BC and bagasse biochar, respectively. The pH_{zpc} of HAP-BC was lower than the pH_{zpc} of cellulose carbonate hydroxylapatite composite and most commercial activated carbons, but higher than the pH_{zpc} of bagasse biochar (De and Ellerbroek 1994; Corapcioglu and Huang 1987).

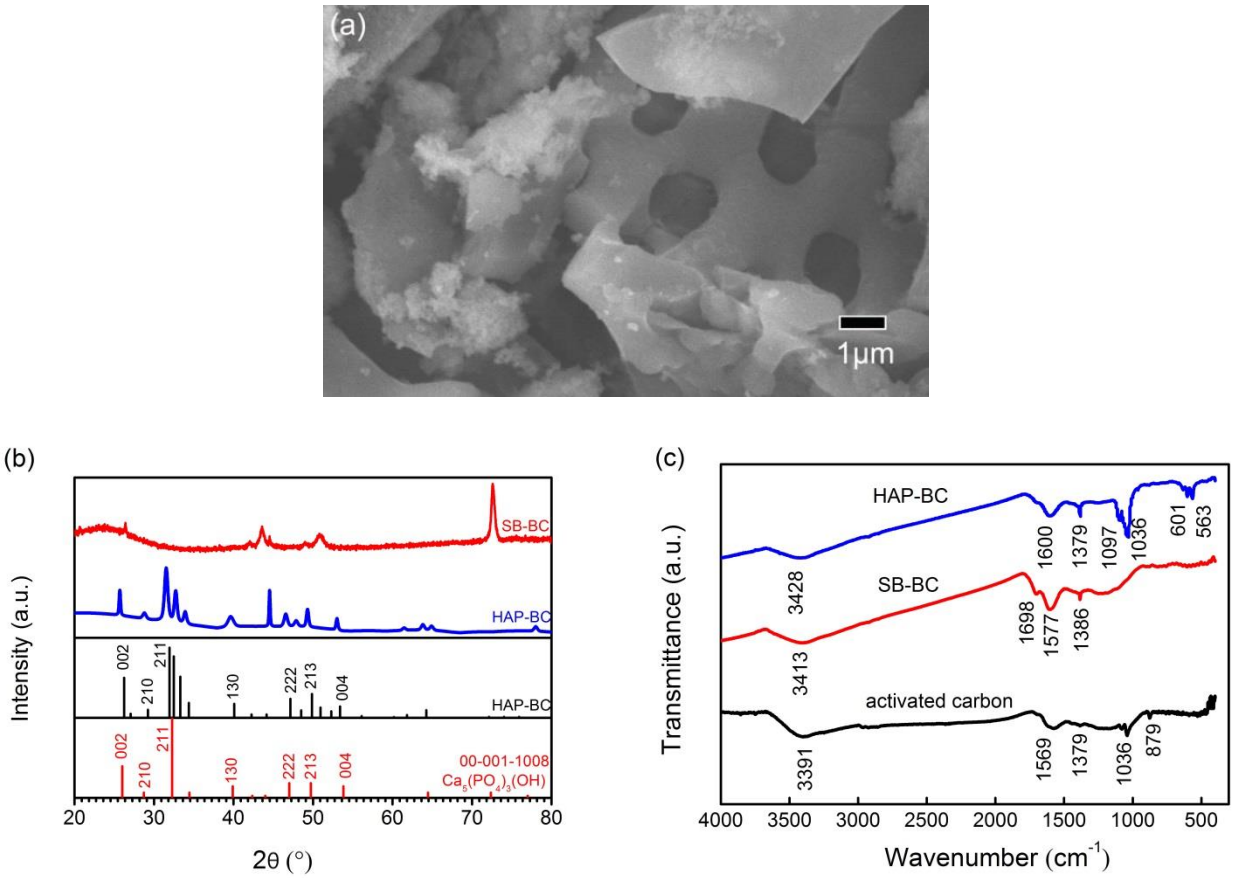

Fig. 2. SEM (a), XRD (b), and FTIR (c) of the HAP-BC

Major Factors Affecting Pb(II) Adsorption

The pH of the wastewater influences the adsorption performance of HAP-BC in terms of Pb(II), as shown in Fig. 3a. At C_0 equal to 100 $mg \cdot L^{-1}$, the Pb(II) adsorption capacity was increased from 24.1 $mg \cdot g^{-1}$ to 49.0 $mg \cdot g^{-1}$ by the pH was increased from 2.0 to 7.0. In addtion, at C_0 equal to 400 $mg \cdot L^{-1}$, the Pb(II) adsorption capacity was increased between 163.7 $mg \cdot g^{-1}$ and 199.2 $mg \cdot g^{-1}$ as the pH was increased from 2.0 to 7.0. In a word, the optimum pH was in the range of 4.0 to 7.0.

In addition, the nature of the surface charge could play a role in Pb(II) adsorption (Sreejalekshmi *et al.* 2009). At a pH less than the pH_{zpc}, the adsorbent surface was positively charged, such that there was a strong electrostatic repulsion between the surface groups and the Pb(II) species (Sreejalekshmi *et al.* 2009). At a pH less than 7.0, the predominant Pb(II) species was Pb^{2+}, with a strong electrostatic repulsion between the positively charged HAP-BC and the cationic Pb(II) species, as expected, which had no benefit to Pb(II) adsorption *via* the HAP-BC. However, the results showed that the optimum pH was in the range from 4.0 to 7.0. Therefore, one can conclude, that additional

forces other than the electrostatic attraction, *e.g.*, dissolution/precipitation and surface complexation, contributed to Pb(II) adsorption (Feng *et al.* 2009).

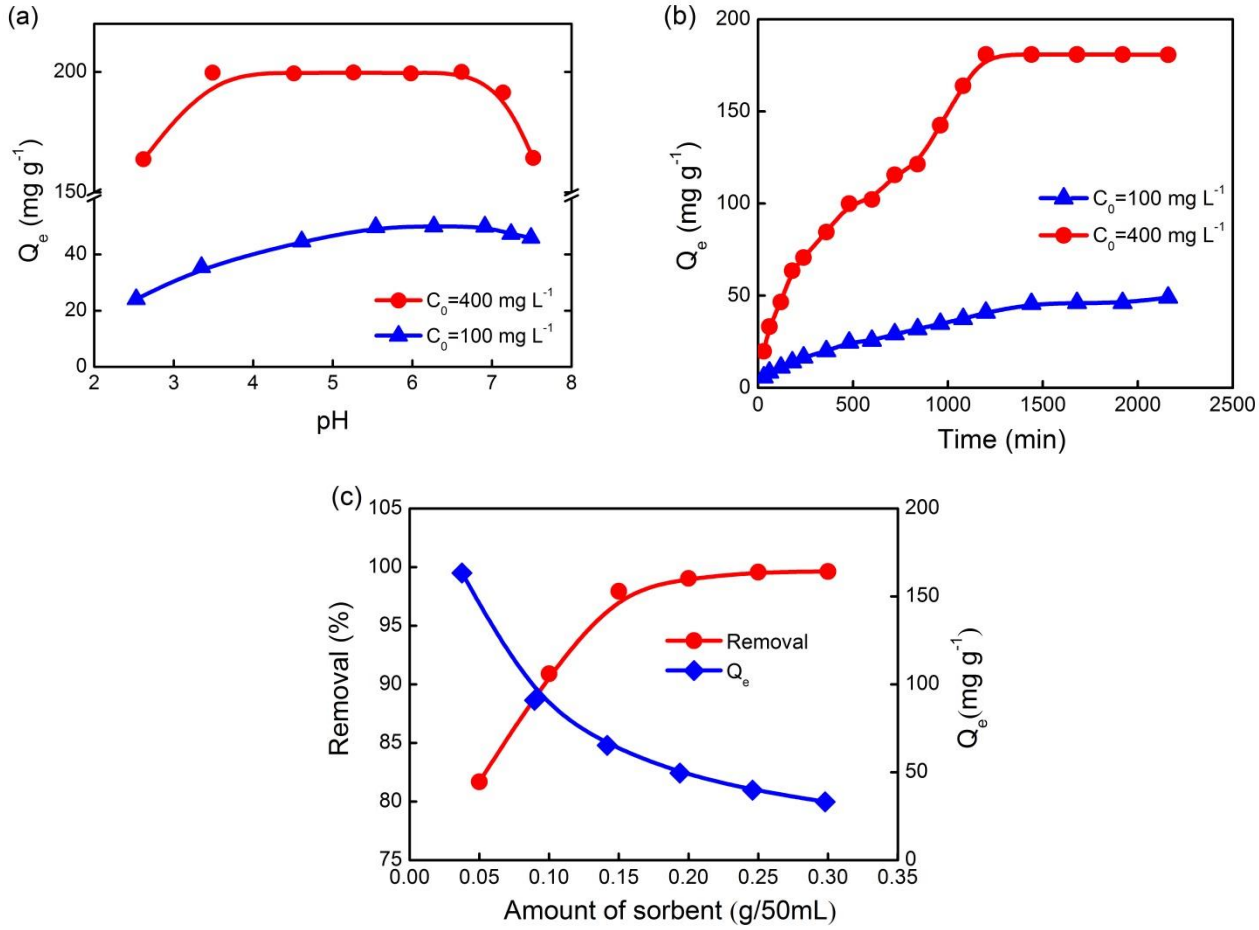

Fig. 3. Major factors affecting the Pb(II) adsorption by HAP-BC: (a) pH, (b) contact time, and (c) adsorbent dose. Experimental conditions: temperature of 25 °C; for (b) the pH was 5.0

The mechanism of dissolution is shown in Eq. 3,

$$Ca_5(PO_4)_3(OH)(s) \rightarrow 5Ca^{2+}+3PO_4^{3-}+OH^- \quad (3)$$

and the precipitation mechanism is shown in Eq. 4,

$$3Pb^{2+}+2PO_4^{3-}+OH^- \rightarrow Pb_3(PO_4)_2(s) \quad (4)$$

After the dissolution of Ca^{2+}, HAP-BC, hydroxyapatite, and Pb (II) formed a more stable lead phosphate, which was more conducive to the removal of Pb^{2+}, while the effect of Ca^{2+} could be ignored ($K_{sp}[Pb_3(PO_4)_2] = 8.0\times10^{-43}$, $K_{sp}[Ca_3(PO_4)_2] = 1.0\times10^{-25}$) (Srinivasan *et al.* 2006; Feng *et al.* 2009).

Table 1 shows the concentration of Ca^{2+}, PO_4^{3-}, and the Ca to P molar ratio at different pHs. There was a decrease in the concentration of Ca^{2+} and PO_4^{3-} as the pH increased from 2.1 to 9.3. In addition, the Ca to P molar ratio increased from 4.5 to 36.8 at an initial Pb(II) concentration of 100 mg·L^{-1}. However, at an initial Pb(II) concentration of 400 mg L^{-1}, the calcium to phosphorus molar ratio in the solution increased from 17.0 to 42.7 within a pH range of 2.1 to 6.8, but decreasing from 42.67 to 16.00 when the pH

increased from 6.8 to 9.3. At a pH less than 6.8, the calcium to phosphorus molar ratio at an initial Pb(II) concentration of 400 mg·L^{-1} was greater than the calcium to phosphorus molar ratio at an initial Pb(II) concentration of 100 mg·L^{-1} at the same pH value, which was far greater than the theoretical Ca to P molar ratio of hydroxylapatite (1.67). It was confirmed that the Pb(II) adsorption mechanism of HAP-BC included ion exchange, dissolution/precipitation, and surface complexation working together (Feng *et al.* 2009).

Table 1. Effect of the pH on Hydroxylapatite Bagasse Biochar Composite (HAP-BC) Ion Concentrations

pH	Calcium Concentration (mmol·L^{-1})		Phosphate Concentration (mmol·L^{-1})		Calcium to Phosphorus Molar Ratio	
	$C_{0(Pb)}$ (mg·L^{-1})		$C_{0(Pb)}$ (mg·L^{-1})		$C_{0(Pb)}$ (mg·L^{-1})	
	100	400	100	400	100	400
2.1	7.12	7.30	1.57	0.43	4.54	16.98
3.1	1.85	4.78	0.46	0.27	4.06	17.70
4.0	1.27	3.69	0.18	0.18	7.24	20.50
5.1	1.06	3.27	0.13	0.08	8.30	40.88
6.1	1.01	2.89	0.09	0.07	10.75	41.29
6.8	0.90	2.56	0.07	0.06	12.80	42.67
7.9	0.73	1.23	0.03	0.05	34.44	24.60
9.3	1.03	1.12	0.03	0.07	36.80	16.00

When the Pb(II) concentration was 100 and 400 mg·L^{-1}, the Pb(II) was sorbed within the first 500 min at average sorption rates of 0.0319 and 0.0754 mg·g^{-1} min^{-1}, respectively. The rapid sorption rate was typical of ion adsorption from aqueous solutions and indicative of favoured interactions between the HAP-BC and Pb(II). The results shown in Fig. 3b also showed that the amount of Pb(II) adsorption reached a plateau at 1200 and 1400 min at the initial Pb(II) concentrations of 100 and 400 mg·L^{-1}, respectively. Mondal *et al.* (2007) reported that the adsorption reaction rapidly occurred during the initial stage, which was followed by a slow reaction until adsorption equilibrium was reached.

When maintaining the contact time, pH, and initial Pb(II) concentration constant at 25 °C, the adsorption of Pb(II) by the HAP-BC was studied by changing the amount of adsorbent in the test solution (Fig. 3c). Increasing the adsorbent dose was attributed to increasing the surface area and availability of additional adsorption sites, but the amount of Pb(II) absorbed per unit mass of the adsorbent decreased from 163.4 to 32.2 mg·g^{-1} as the adsorbent dose increased. The percentage of Pb(II) removed from the solution increased from 81.9% to 99.6% as the HAP-BC dosage increased from 0.05 to 0.30 g in a 50 mL solution. At the same time, the pH of the solution at adsorption equilibrium decreased from 4.26 to 4.16 as the HAP-BC dose increased from 0.05 g to 0.30 g in a 50 mL solution.

Adsorption Isotherm

The Pb(II) adsorption isotherm is shown Fig. 4, in which SB-BC and HAP-BC are at a different temperature. At a temperature of 25, 35 and 45 °C, the Pb(II) adsorption capacity quickly increased as the equilibrium Pb(II) concentration increased when it was lesser than 20 mg·L^{-1}. The Pb(II) adsorption capacity slowly increased when the equilibrium Pb(II) concentration increased when it was greater than 20 mg·L^{-1}. The equilibrium adsorption capacity of HAP-BC to Pb(II) at temperatures of 25, 35, and 45 °C were 193, 202, and 206 mg·g^{-1}, respectively. It was interesting to note that HAP-BC exhibited a Pb(II) adsorption capacity thirty times that of SB-BC.

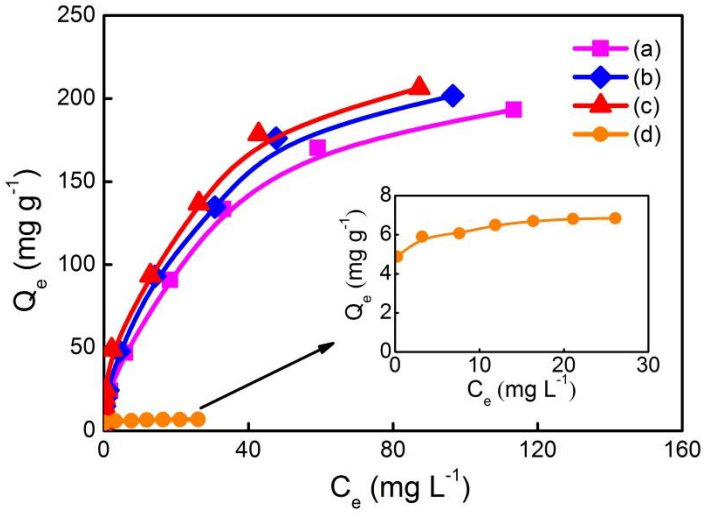

Fig. 4. Langmuir adsorption isotherm of Pb(II) on HAP-BC at different temperature (pH = 5.0): (a) HAP-BC adsorbed Pb(II) at 25 °C; (b) HAP-BC adsorbed Pb(II) at 35 °C; (c)HAP-BC adsorbed Pb(II) at 45 °C; and (d) SB-BC adsorbed Pb(II) at 25 °C

The Pb(II) adsorption density can be well described by the Langmuir adsorption isotherm shown in Eq. 5,

$$q = \frac{q_{\max} C_e K_L}{1 + C_e K_L} \quad (5)$$

where q is the adsorption density (mg·g^{-1}), q_{max} is the monolayer-layer adsorption density (mg·g^{-1}), K_L is the Langmuir constant (M^{-1}), and C_e is the equilibrium concentration (as shown in Fig. S3).

The data were found to fit Eq. 5, with a coefficient of determination (R^2) of 0.980, 0.981, and 0.980, at a temperature of 25, 35, and 45 °C, respectively. In addition, the adsorption capacity increased from 210 mg·g^{-1} (at 25 °C) to 216 mg·g^{-1} (at 45 °C) (as shown in Table 2).

Table 2. Langmuir Isotherms Parameters for Pb(II) Adsorption by Hydroxylapatite Bagasse Biochar Composite (HAP-BC)

Item	q_m (mg·g^{-1})	K_L (M^{-1})	R^2	ΔG (kJ·mol^{-1})
SB-BC (25 °C)	6.94	4.90×10^{-7}	0.999	-39.49
HAP-BC (25 °C)	209.6	1.68×10^{-6}	0.980	-35.53
HAP-BC (35 °C)	213.7	1.72×10^{-6}	0.981	-36.78
HAP-BC (45 °C)	216.5	2.88×10^{-6}	0.980	-39.34

These results indicated that the Pb(II) adsorption by HAP-BC was an endothermic reaction. In addition, HAP-BC exhibited a Pb(II) adsorption capacity of 210 mg·g^{-1}, which was greater than the Pb(II) adsorption capacity of sorghum biochar (17.8 mg·g^{-1}), and it was four times greater than the Pb(II) adsorption capacity of bamboo biochar (55.6 mg·g^{-1}) (Wang *et al.* 2012). Compared to other literature (Naushad 2014; Naushad *et al.* 2014; Naushad *et al.* 2015), the comparison of maximum monolayer adsorption capacities (Q_m) of Pb(II) ion on different adsorbents are given in Table 3.

Table 3. Comparison of Maximum Monolayer Adsorption Capacity of Pb(II) ion using Various Adsorbents

Adsorbents	Maximum monolayer adsorption capacity Q_m (mg g^{-1})	References
corn straws graphene oxide biochar	26.1	Zhang *et al*. 2018
cotton stalk-derived biochar	147	Gao *et al*. 2021
canola straw biochar	165	Nzediegwu *et al*. 2021
KH_2PO_4-modified biochar	154.7	Xu *et al*. 2021
sludge-based biochar	16.70	Zhang *et al*. 2018
canola straw biochar	108	Kwak *et al*. 2019
wheat straw biochar	109	Kwak *et al*. 2019
bean-worm skin biochar	62	Yan *et al*. 2020
mild air oxidation biochar	44	Bardestani *et al*. 2019
Enteromorpha biochar	98	Yang *et al*. 2019
corncob biochar based montmorillonite composite	140	Fu *et al*. 2020
hydroxylapatite bagasse biochar	216	Present work

However, the Pb(II) adsorption capacity of HAP-BC was much greater than the Pb(II) adsorption capacity of SB-BC at a temperature of 25 °C (7.04 mg·g^{-1}). The K_L values were 1.68×10^{-6}, 1.72×10^{-6}, and 2.88×10^{-6} M^{-1} at 25, 35, and 45 °C, respectively. The change in the Gibbs free energy (ΔG) of the HAP-BC adsorption of Pb(II) can be calculated from the Nernst equation, as shown in Eq. 6,

$$\Delta G = RT \ln K_L \quad (6)$$

where R is the gas constant (8.314 J $mol^{-1}\cdot K^{-1}$) and T is the absolute temperature (K). The ΔG (as shown in Table 2) indicated the spontaneous nature of Pb(II) adsorption by HAP-BC.

Adsorption Kinetics

Among different kinetic models, the experimental data could be best fit to the internal-particle diffusion kinetic model. According to the intra-particle diffusion model proposed by Weber–Morris (Naushad 2014; Naushad *et al*. 2014), the root time dependence may be expressed as Eq. 7,

$$q_t = k_i t^{1/2} \quad (7)$$

where q_t is the adsorption capacity of HAP-BC at time t (mg·g^{-1}), t is the time (min), and k_i is the intraparticle diffusion rate constant (mg·$g^{-1}\cdot min^{-1/2}$) (Crini 2008).

When the Pb(II) concentrations were 100 and 200 mg·L^{-1}, the intra-particle diffusion rate constants k_i were 1.14 mg·$g^{-1}\cdot min^{-1/2}$ and 2.13 mg·$g^{-1}\cdot min^{-1/2}$ and the correlation coefficients were 0.996 and 0.982, respectively (as shown in Fig. S4 and Table 4). This indicated that the intra-particle diffusion kinetic model was suitable in terms of fitting the HAP-BC adsorption kinetics process of Pb(II), and the intra-particle diffusion process controls the primary steps of the adsorption of Pb(II) by HAP-BC.

Table 4. Kinetic Parameters of Pb(II) Sorption by Hydroxylapatite Bagasse Biochar Composite (HAP-BC)

Pb(II) Concentration ($mg \cdot L^{-1}$)	k_i ($mg \cdot g^{-1} \cdot min^{-1/2}$)	R^2
100.0	1.14	0.996
200.0	2.31	0.982

Potential Adsorption Mechanism

The X-ray diffraction analysis showed an obvious structural change (as shown in Fig. 5). The major carbon peaks were at 44.54°, which disappeared after Pb(II) adsorption occurred, which may be because the degree of crystallization of the organic charcoal in the bagasse carbonization product is lower. The major characteristic peaks (2θ) of HAP-BC were shifted to a lower diffraction angle after Pb(II) adsorption occurred, compared with the major characteristic peaks before Pb(II) adsorption at 31.78°, 39.83°, 46.68°, and 53.55°, which was likely due to the complex adsorption reaction between HAP-BC and Pb(II). The diffraction peaks of lead hydroxylapatite (Reference code 00-001-0924) were recognized in the HAP-BC after Pb(II) adsorption occurred, which indicated that dissolution/precipitation and ion exchange reactions during the Pb(II) adsorption process by HAP-BC occurred. This may be the reason the solubility product constants of lead phosphate are much smaller than the solubility product constants of calcium phosphate ($K_{sp}[Pb_3(PO_4)_2] = 8.0\times10^{-43}$ versus $K_{sp}[Ca_3(PO_4)_2] = 1.0\times10^{-25}$), and consequently, accompanied by the dissolution of HAP-BC, a more stable lead phosphate was formed (Srinivasan *et al.* 2006; Feng *et al.* 2009).

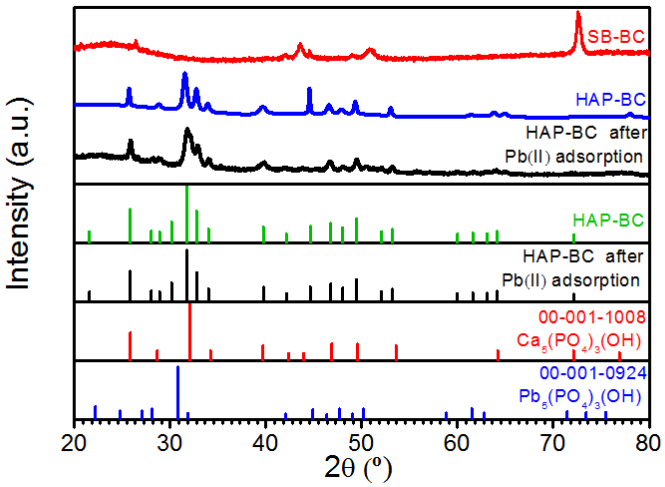

Fig. 5. XRD spectrogram of the HAP-BC before and after Pb(II) adsorption

To better understand the Pb(II) adsorption mechanism by HAP-BC, the amounts of Pb(II) adsorbed and the Ca^{2+} concentration, as well as the pH variation after adsorption, were measured by the adsorption isotherm experiments, as shown in Fig. 6a and 6b. It can be seen from Fig. 6 that the molar concentration of the released Ca^{2+} was not equal to the molar Pb(II) uptake by HAP-BC as the initial Pb(II) concentration and the amounts of Pb(II) adsorbed increased. In addition, the difference between the amounts of Pb(II) adsorbed and Ca^{2+} released became larger as the initial Pb(II) concentration and the amounts of Pb(II) adsorbed increased, which suggested that the Pb(II) adsorption process may also be affected by other factors outside of dissolution and precipitation.

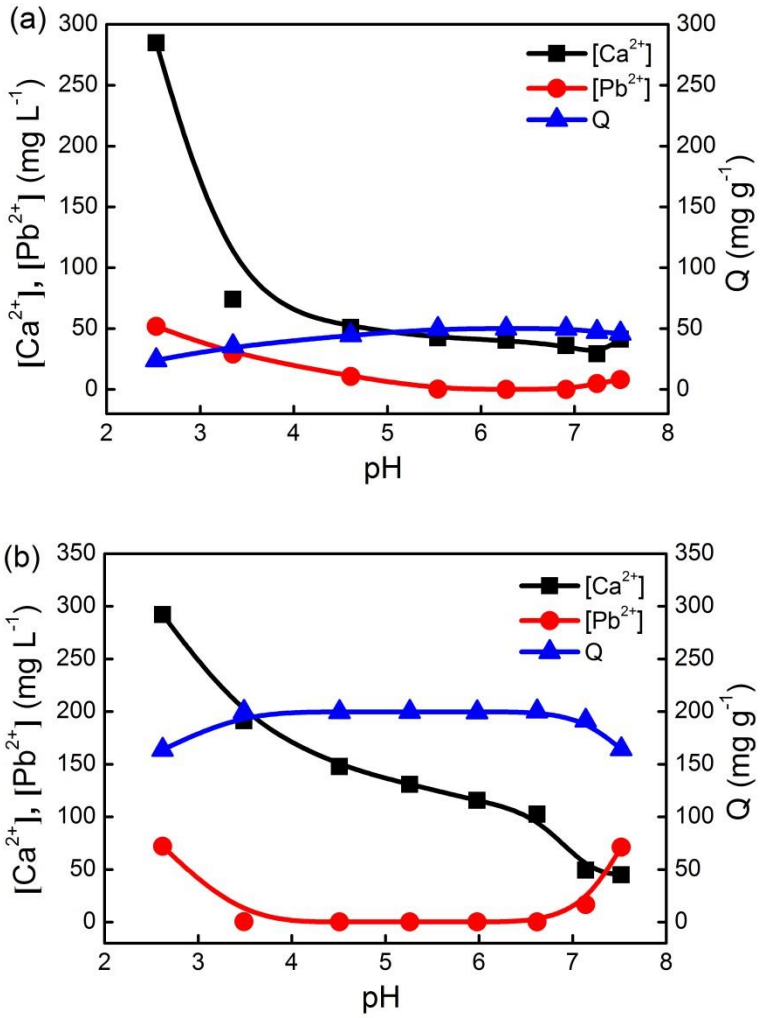

Fig. 6. The pH variation after adsorption was monitored *via* the adsorption of Ca^{2+}, Pb^{2+}, and Q_e versus the pH: (a) $C_{0(Pb)}$ = 100 mg·L^{-1}; and (b) $C_{0(Pb)}$ = 400 mg·L^{-1}

The XPS survey spectra of the HAP-BC and the HAP-BC after Pb(II) adsorption are shown in Fig. 7a. The observed photoelectron signals were C1s (276 eV to 290 eV), O1s (522 eV to 536 eV), Ca2p (340 eV to 355 eV), and P2p (125 eV to 145 eV). Phosphor constituted only accounted for 18.5% of the HAP chemical composition and its XPS sensitivity factor was relatively low, *i.e.*, 22 (Moulder *et al.* 1995). The peak centered at 138.13 and 142.95 eV (the HAP-BC spectrum after Pb(II) adsorption) was due to the $Pb4f_{7/2}$ and $Pb4f_{5/2}$. The doublets characteristic of Pb in HAP-BC after Pb(II) adsorption appeared at 138.13 eV (assigned to Pb $4f_{7/2}$) and at 142.95 eV (assigned to Pb $4f_{5/2}$); the peak observed at 138.13 eV agrees with the 138.4 eV value reported for $Pb(OH)_2$ by Lee *et al.* (2006), which indicated further complexation of Pb by HAP-BC and the precipitation of Pb.

The atomic concentration (at.%) of the adsorbent surface elements, as detected by XPS, was determined for the HAP-BC before and after Pb(II) adsorption (as shown in Fig. 7b). The amounts of O, Ca, P, and Pb significantly increased after Pb(II) adsorption by HAP-BC, which revealed that the variation in the XPS analysis area was due to the ill-defined porous structure of the resorbing HAP-BC layer. However, the amounts of O, Ca, P, and Pb detected on the HAP-BC samples were observed to be less than the amounts of

O, Ca, P, and Pb detected on the HAP-BC samples after Pb(II) adsorption. This may also be explained by the variation in the XPS analysis area due to the ill-defined porous structure of the resorbing HAP-BC layer.

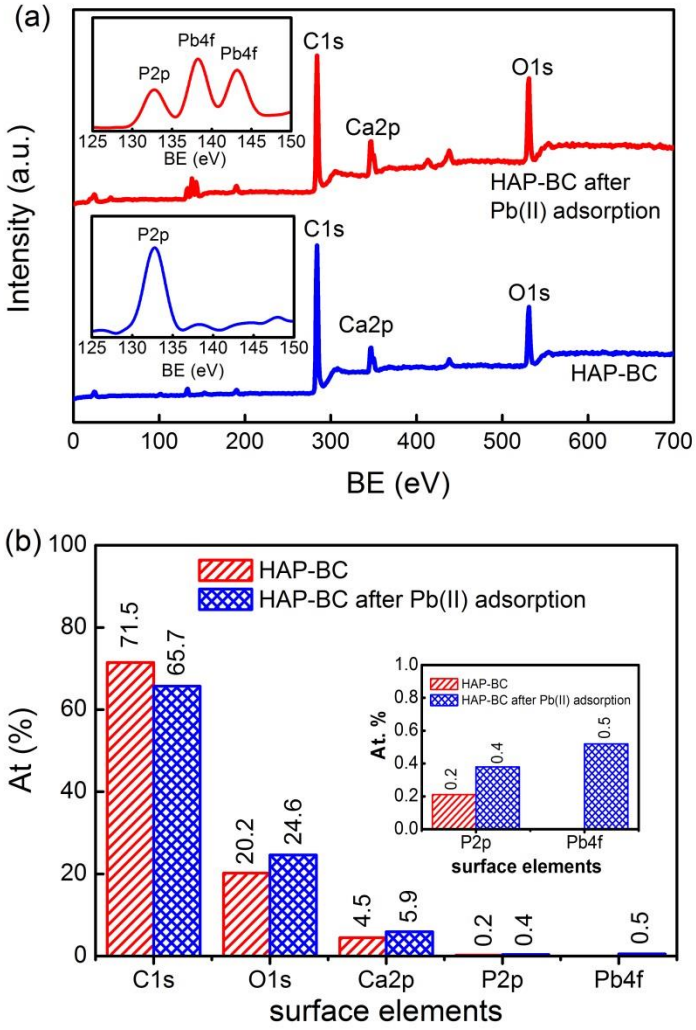

Fig. 7. XPS of the: (a) full spectrogram; and (b) Atomic concentration of the surface elements of the HAP-BC before and after Pb(II) adsorption

The XPS spectra of the O1s and C1s orbitals are shown in Figs. 8a, 8a', 8b, and 8b'. The high-resolution XPS C1s spectra are shown in Figs. 8a and 8a'.

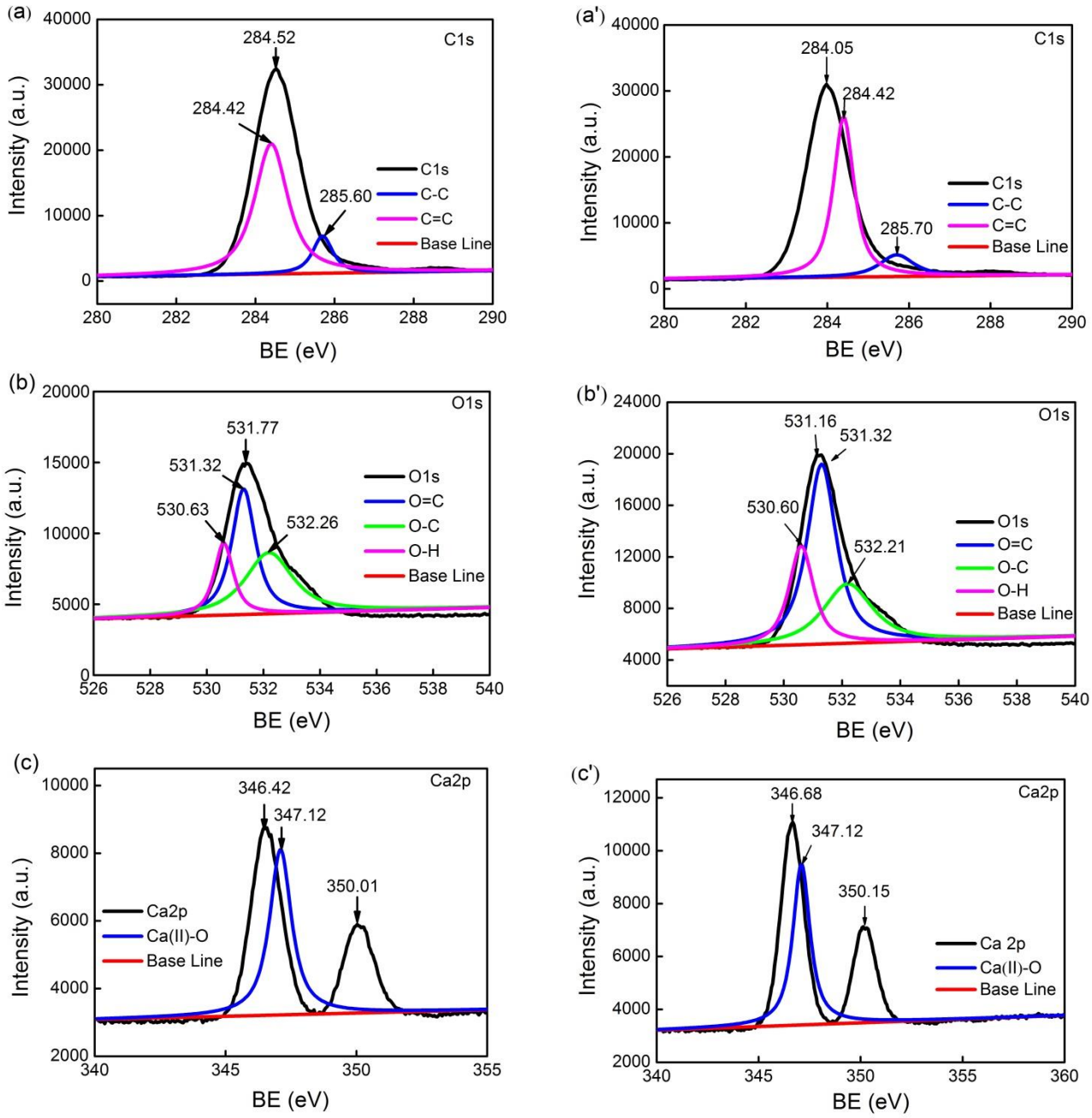

Fig. 8. XPS sub-peak fitted spectra of HAP-BC before and after Pb(II) adsorption: (a) C1s of HAP-BC; (a') C1s of HAP-BC after Pb(II) adsorption; (b) O1s of HAP-BC; (b') O1s of HAP-BC after Pb(II) adsorption; (c) Ca2p of HAP-BC; and (c') Ca2p of HAP-BC after Pb(II) adsorption

The peak of typical graphitic carbon at 284.52 and 284.05 eV represents the C1s binding energy of the HAP-BC before and after Pb(II) adsorption, respectively. The C1s peak was shifted by 0.47 eV, suggesting that the species of carbon is influenced by Pb(II); no shift in the XPS spectra of C-C and C=C suggested that carbon was not involved in the adsorption process. Figures 8b and 8b' show that the primary O1s peak was shifted from 531.77 to 531.16 eV after Pb(II) adsorption, *i.e.*, the oxygen peak was shifted by 0.61 eV. This shift may be due to $Pb_5(PO_4)_3(OH)$ pellets beginning to form and cover the adsorbent surface of the HAP-BC. Results showed the presence of oxygen-containing functional

groups on the surface of HAP-BC in the form of carbonyl oxygen, *i.e.*, -O=C, (530.6 eV), hydroxyl, *i.e.*, -O-H, (531.32 eV), and carboxyl oxygen, *i.e.*, -O-C, (532.26 eV) (Zhang *et al.* 2010). The Pb(II) adsorption was accompanied by a change in oxygen binding, which provided evidence that the oxygen-containing functional groups on the surface of HAP-BC took part in the Pb(II) adsorption process. The bonding energy of Ca2p increased from 346.42 to 346.68 eV after the Pb(II) adsorption by HAP-BC; these values were typical for Ca^{2+} in hydroxylapatite (as shown in Fig. 8c and 8c').

The change in bonding energy was illustrated by the electron transfer in the valence band, as well as the actual charge transfers, due to chemical reactions. Accordingly, by tracking the change in the core level peak position of the substrate, with and without the formation of surface complexes, it was possible to deduce the direction of the electron transfer during adsorption as well as to assess the relative acidity and basicity of the substrate and evaluate the adsorbate (Ding *et al.* 2000). The O1s binding energy and intensity shift were dependent on the content of different oxygen atoms, especially on the surface of HAP-BC. A simple formula connecting the O1s chemical shift and charge was constructed using the frontier molecular orbital theory as the theoretical framework, as shown in Eq. 8,

$$Q_0 = -4.372 + \frac{[385.023 - 8.976 \times (545.509 - O1sBE)^{1/2}}{4.488} \quad (8)$$

where Q_0 is the actual oxygen charge in the adsorbent (esu) and O1sBE is the O1s binding energy determined *via* XPS (eV).

According to Eq. 8, the charge of the oxygen on the HAP-BC surface before and after Pb(II) adsorption were -0.84 and -0.80 esu, respectively (as shown in Table 5). This indicated the actual charge of oxygen was insignificantly changed, and Pb(II) adsorption by HAP-BC did not involve noticeable electron transfer between the HAP-BC surface and Pb(II) after the Pb(II) adsorption process. Since the actual transferred charge amount was 0.04 esu, which is less than 1 esu, the outer shared electronics of the oxygen atom on the surface the HAP-BC may be offset during the bond formation process (Ding *et al.* 2000). The oxygen from HAP-BC acts as a Lewis base, while various Pb(II) ions in the aqueous solution act as a Lewis acid (Ding *et al.* 2000).

Table 5. Oxygen (1s) Binding Energies, Charge Changes, and Electron Transfer Direction for the Hydroxylapatite Bagasse Biochar Composite (HAP-BC) Before and After Pb(II) Adsorption

Compound	Binding Energy (eV)	Charges (esu)	Electron Transfer Direction
HAP-BC	530.63	-0.84	-
After Pb(II) adsorption	531.25	-0.80	Electron donor

The XPS spectra of the Pb4f, $Pb4f_{5/2}$, and $4f_{7/2}$ orbitals are shown in Fig. S5, which demonstrated that the Pb4f peak was at 138.8 eV, the $Pb4f_{5/2}$ peak was at 138.9 eV, and the $Pb4f_{7/2}$ peak was at 143.8 eV. The shift of the Pb4f orbital spectra at a binding energy (BE) of 143.8 eV after Pb(II) absorption clearly demonstrated that the oxygen-containing functional groups were involved in the adsorption reaction, and that hydroxylapatite played a significant role in Pb(II) adsorption.

Engineering Implications

The mining wastewater was adsorbed by HAP-BC, which had initial concentrations of arsenic, lead, zinc, and cadmium in the mining wastewater of 0.39, 0.26, 3.55, and 2.16 $mg \cdot g^{-1}$, respectively. At a pH of 9.0, the removal percentage of arsenic, lead, zinc, and cadmium by HAP-BC were 88.83%, 100.00%, 99.89%, and 99.68%, respectively (as shown in Table 6). The removal of lead, cadmium, and zinc by HAP-BC was greater than the removal of arsenic at a pH of 5.0, 7.0, and 9.0. As such, HAP-BC can efficiently treat complex Pb(II)-containing wastewater.

Table 6. Experimental Results of Adsorption of Mining Wastewater by Hydroxylapatite Bagasse Biochar Composite (HAP-BC)

pH	Removal (%)				Residual Concentration ($mg \cdot L^{-1}$)			
	Arsenate	Lead	Zinc	Cadmium	Arsenate	Lead	Zinc	Cadmium
5.0	80.83	100.00	82.70	85.89	0.074	-	0.62	0.30
7.0	85.28	100.00	92.26	98.93	0.057	-	0.28	0.02
9.0	88.83	100.00	99.89	99.68	0.043	-	0.00	0.01

Results show the benefits of HAP-BC as an adsorbent for the removal of Pb(II) in water. From the view of engineering process applications, the adsorbent has three major attributes. First, the HAP particles contribute to the considerable specific surface area of the HAP-BC, which provides abundant surface sites necessary for heavy metal ion adsorption.

Second, the bagasse support allows for the design of the metal removal processes to operate in a fixed bed mode, which can greatly reduce the post-metal treatment costs of particle separation. Finally, the pH-dependent nature of the metal adsorption process permits easy regeneration of the saturated adsorbent. It is feasible to regenerate the HAP-BC when it reaches maximum adsorption capacity.

In actuality, at a pH of less than 2 or greater than 9, the Pb(II) ions are easy to desorb from the surface of HAP-BC. In addition, it was easy to recover the Pb(II) from regenerating solutions because the Pb(II) concentration was high in those solutions.

Reusability

Figure 9 shows the differences in Pb(II) removal to estimate the reusability of the SB-BC and HAP-BC after 4 adsorption/desorption cycles. As such, the SB-BC and HAP-BC were washed with a 2.1% HCl solution after the adsorption of Pb(II), oven-dried, and then recycled for Pb(II) removal. The results showed that there was difference in the Pb(II) removal percentage between SB-BC and HAP-BC after washing with acid. In first cycle, the Pb(II) removal percentage by SB-BC and HAP-BC were 57.21% and 95.67%, respectively, while after the 4^{th} cycle it changed to 51.76% and 92.52%, respectively. The difference in the Pb(II) removal percentage was 5.45% and 3.15%, respectively. As such, HAP-BC had greater reusability than SB-BC in terms of removing Pb(II) from contaminated water.

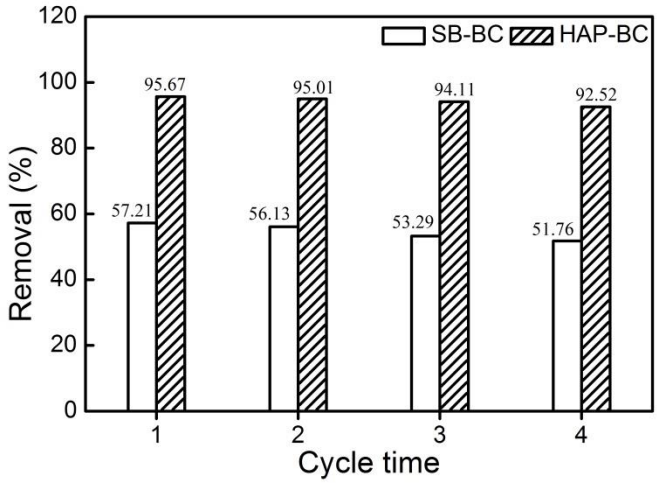

Fig. 9. The reusability of SB-BC and HAP-BC for the removal of Pb(II)

CONCLUSIONS

1. From the results obtained, the optimum pH for Pb(II) adsorption by HAP-BC was between 4.0 and 7.0. The maximum adsorption capacity of Pb(II) by HAP-BC, as calculated by the Langmuir isotherm, was 210 mg g^{-1} at 25°C.
2. The removal mechanism of Pb(II) by HAP-BC in solution was primarily by surface diffusion, electrostatic attraction, surface complexation, ion exchange, and a dissolving coprecipitation reaction.
3. The oxygen-containing functional groups, *i.e*., O=C, O-C, and O-H, of HAP-BC were involved in adsorbing Pb(II). The shift of the Pb4f orbital spectra at a binding energy (BE) of 143.84 eV after the Pb(II) absorption process by HAP-BC demonstrated that the surface oxygen-containing functional groups were involved in the adsorption reaction.
4. The HAP-BC was used to treat complex water bodies containing arsenic, zinc, and cadmium, and its removal rate of lead was as much as 100%, which suggests it is a promising environmentally friendly functional material and can be used in environmental pollution control.

ACKNOWLEDGEMENTS

This research was financially assisted by the National Natural Science Foundation of China (No. 21367010 and No. 51638006) and the Guangxi Mid-Youth Capability Project (No. 2020KY06038).

REFERENCE CITED

Argun, M. E., Dursun, S., Ozdemir, C., and Karatas, M. (2007). "Heavy metal adsorption by modified oak sawdust: Thermodynamics and kinetics," *Journal of Hazardous Materials* 141(1), 77-85. DOI: 10.1016/j.jhazmat.2006.06.095

Bardestani, R., Roy, C., and Kalioguine, S. (2019). "The effect of biochar mild air oxidation on the optimization of lead(II) adsorption from wastewater," *Journal of Environmental Management* 240, 404-420. DOI: 10.1016/j.jenvman.2019.03.110

Chand, P., and Pakade, Y. B. (2015). "Synthesis and characterization of hydroxyapatite nanoparticles impregnated on apple pomace to enhanced adsorption of Pb(II), Cd(II), and Ni(II) ions from aqueous solution," *Environmental Science and Pollution Research* 22(14), 10919-10929. DOI: 10.1007/s11356-015-4276-2

Corami, A., Mignardi, S., and Ferrini, V. (2008). "Cadmium removal from single- and multi-metal (Cd + Pb + Zn + Cu) solutions by sorption on hydroxyapatite," *Journal of Colloid and Interface Science* 317(2), 402-408. DOI: 10.1016/j.jcis.2007.09.075

Corapcioglu, M. O., and Huang, C. P. (1987). "The surface acidity and characterization of some commercial activated carbons," *Carbon* 25(4), 569-578. DOI: 10.1016/0008-6223(87)90200-4

Crini, G. (2005). "Recent developments in polysaccharide-based materials used as adsorbents in wastewater treatment," *Progress in Polymer Science* 30(1), 38-70. DOI: 10.1016/j.progpolymsci.2004.11.002

Crini, G. (2008). "Kinetic and equilibrium studies on the removal of cationic dyes from aqueous solution by adsorption onto a cyclodextrin polymer," *Dyes and Pigments* 77(2), 415-426. DOI: 10.1016/j.dyepig.2007.07.001

De, J. B. H. W. S., and Ellerbroek, D. (1994). "Low-temperature structure of lithium nesosilicate, Li_4SiO_4, and its Li_{1s} and O_{1s} x-ray photoelectron spectrum," *Acta Crystallographica* 50(5), 511-518. DOI: 10.1107/S0108768194002375

Ding, M., Jong, B. H. W. S. d., Roosendaal, S. J., and Vredenberg, A. (2000). "XPS studies on the electronic structure of bonding between solid and solutes: adsorption of arsenate, chromate, phosphate, Pb^{2+}, and Zn^{2+} ions on amorphous black ferric oxyhydroxide," *Geochimica et Cosmochimica Acta* 64(7), 1209-1219. DOI: 10.1016/S0016-7037(99)00386-5

Elouear, Z., Bouzid, J., Boujelben, N., Feki, M., Jamoussi, F., and Montiel, A. (2008). "Heavy metal removal from aqueous solutions by activated phosphate rock," *Journal of Hazardous Materials* 156(1), 412-420. DOI: 10.1016/j.jhazmat.2007.12.036

Feng, N., Guo, X., and Liang, S. (2009). "Adsorption study of copper (II) by chemically modified orange peel," *Journal of Hazardous Materials* 164(2), 1286-1292. DOI: 10.1016/j.jhazmat.2008.09.096

Fu, C.-L., Zhang, H.-L., Xia, M.-Z., Lei, W., and Wang, F.-Y. (2020). "The single/co-adsorption characteristics and microscopic adsorption mechanism of biochar-montmorillonite composite adsorbent for pharmaceutical emerging organic contaminant atenolol and lead ions," *Ecotoxicology and Environmental Safety* 187, article no. 109763. DOI: 10.1016/j.ecoenv.2019.109763

Gao, L., Li, Z.-H., Yi, W.-M., Li, Y.-F., Zhang, P., Zhang, A.-D., and Wang, L.-H. (2021). "Impacts of pyrolysis temperature on lead adsorption by cotton stalk-derived biochar and related mechanisms," *Journal of Environmental Chemical Engineering* 9, article no. 105602. 10.1016/j.jece.2021.105602

Gupta, N., Kushwaha, A. K., and Chattopadhyaya, M. C. (2012). "Adsorptive removal of

Pb^{2+}, Co^{2+} and Ni^{2+} by hydroxyapatite/chitosan composite from aqueous solution," *Journal of the Taiwan Institute of Chemical Engineers* 43(1), 125-131. DOI: 10.1016/j.jtice.2011.07.009

Jayakodiarachchi, N., and Jayaweera, C. D. (2015). "A study of the removal characteristics of Cu (ii) ions from aqueous solutions by a low-cost adsorbent," in *Proceedings of the 20th International Forestry and Environment Symposium*, 16-17 October, Waikkal, Sri Lanka.

Kloss, S., Zehetner, F., Dellantonio, A., Hamid, R., Ottner, F., Liedtke, V., Schwanninger, M., Gerzabek, M. H., and Soja, G. (2012). "Characterization of slow pyrolysis biochars: Effects of feedstocks and pyrolysis temperature on biochar properties," *Journal of Environmental Quality* 41(4), 990-1000. DOI: 10.2134/jeq2011.0070

Kwak, J.-H., Islam, M. S., Wang, S.-Y., Messele, S. A., Naeth, M. A., El-Din, M. G., and Chang, S. X. (2019). "Biochar properties and lead(II) adsorption capacity depend on feedstock type, pyrolysis temyanperature, and steam activation," *Chemosphere* 231, 393-404. DOI: 10.1016/j.chemosphere.2019.05.128

Lee, S., Dyer, J. A., Sparks, D. L., Scrivner, N. C., and Elzinga, E. J. (2006). "A multi-scale assessment of Pb(II) sorption on dolomite," *Journal of Colloid and Interface Science* 298(1), 20-30. DOI: 10.1016/j.jcis.2005.12.022

Liang, M., Wang, D., Zhu, Y., Zhu, Z., Li, Y., and Huang, C. P. (2018). "Nano-hematite bagasse composite (n-HBC) for the removal of Pb(II) from dilute aqueous solutions," *Journal of Water Process Engineering* 21, 69-76. DOI: 10.1016/j.jwpe.2017.11.014

Liu, P., Liu, W.J., Jiang, H., Chen, J.J., Li, W.W., and Yu, H.Q. (2012). "Modification of bio-char derived from fast pyrolysis of biomass and its application in removal of tetracycline from aqueous solution," *Bioresource Technology* 121, 235-240. DOI: 10.1016/j.biortech.2012.06.085.

Meski, S., Ziani, S., and Khireddine, H. (2010). "Removal of lead ions by hydroxyapatite prepared from the egg shell," *Journal of Chemical & Engineering Data* 55(9), 3923-3928. DOI: 10.1021/je901070e

Mondal, P., Balomajumder, C., and Mohanty, B. (2007). "A laboratory study for the treatment of arsenic, iron, and manganese bearing ground water using Fe^{3+} impregnated activated carbon: Effects of shaking time, pH and temperature," *Journal of Hazardous Materials* 144(1), 420-426. DOI: 10.1016/j.jhazmat.2006.10.078

Naushad, M. (2014). "Surfactant assisted nano-composite cation exchanger: Development, characterization and applications for the removal of toxic Pb^{2+} from aqueous medium," *Chemical Engineering Journal* 235, 100-108. DOI: 10.1016/j.cej.2013.09.013

Naushad, M., Alothman, Z. A., Awual, M. R., and Mezbaul Alam, M. (2015). "Adsorption kinetics, isotherms, and thermodynamic studies for the adsorption of Pb^{2+} and Hg^{2+} metal ions from aqueous medium using Ti(IV) iodovanadate cation exchanger," *Ionics* 21, 2237-2245. DOI: 10.1007/s11581-015-1401-7

Naushad, M., Mittal, A., Rathore, M., and Gupta, V. (2014). "Ion-exchange kinetic studies for Cd(II), Co(II), Cu(II), and Pb(II) metal ions over a composite cation exchanger," *Desalination and Water Treatment* 1-8. DOI: 10.1080/19443994.2014.904823

Nzediegwu, C., Naeth, M. A., and Chang, S. X. (2021). "Lead(II) adsorption on microwave-pyrolyzed biochars and hydrochars depends on feedstock type and production temperature," *Journal of Hazardous Materials* 412, article no. 125255. DOI: 10.1016/j.jhazmat.2021.125255

Saber-Samandari, S., Saber-Samandari, S., Nezafati, N., and Yahya, K. (2014). "Efficient

removal of lead (II) ions and methylene blue from aqueous solution using chitosan/Fe-hydroxyapatite nanocomposite beads," *Journal of Environmental Management* 146, 481-490. DOI: 10.1016/j.jenvman.2014.08.010

Satyanarayana, K. G., Guimarães, J. L., and Wypych, F. (2007). "Studies on lignocellulosic fibers of Brazil. Part I: Source, production, morphology, properties and applications," *Composites Part A: Applied Science and Manufacturing* 38(7), 1694-1709. DOI: 10.1016/j.compositesa.2007.02.006

Sreejalekshmi, K. G., Krishnan, K. A., and Anirudhan, T. S. (2009). "Adsorption of Pb(II) and Pb(II)-citric acid on sawdust activated carbon: Kinetic and equilibrium isotherm studies". *Journal of Hazardous Materials* 161(2), 1506-1513. DOI: 10.1016/j.jhazmat.2008.05.002.

Srinivasan, M., Ferraris, C., and White, T. (2006). "Cadmium and lead ion capture with three dimensionally ordered macroporous hydroxyapatite," *Environmental Science & Technology* 40(22), 7054-7059. DOI: 10.1021/es060972s

Wang, Y., Wang, X., Wang, X., Liu, M., Yang, L., Wu, Z., Xia, S., and Zhao, J. (2012). "Adsorption of Pb(II) in aqueous solutions by bamboo charcoal modified with $KMnO_4$ via microwave irradiation," *Colloids and Surfaces A: Physicochemical and Engineering Aspects* 414, 1-8. DOI: 10.1016/j.colsurfa.2012.08.007

Xu, D., Tan, X., Chen, C., and Wang, X. (2008). "Removal of Pb(II) from aqueous solution by oxidized multiwalled carbon nanotubes," *Journal of Hazardous Materials* 154(1), 407-416. DOI: 10.1016/j.jhazmat.2007.10.059

Xu, Y.-G., Bai, T.-X., Li, Q., Yang, H.-T., Yan, Y.-B., Sarkar, B., Lam, S. S., and Bolan, N. (2021). "Influence of pyrolysis temperature on the characteristics and lead(II) adsorption capacity of phosphorus-engineered poplar sawdust biochar," *Journal of Analytical and Applied Pyrolysis* 154, article no. 105010. DOI: 10.1016/j.jaap.2020.105010

Yan, Y., Dong, X., Sun, X., Sun, X., Li, J., Shen, J., Han, W., Liu, X., and Wang, L. (2014). "Conversion of waste FGD gypsum into hydroxyapatite for removal of Pb^{2+} and Cd^{2+} from wastewater," *Journal of Colloid and Interface Science* 429, 68-76. DOI: 10.1016/j.jcis.2014.05.010

Yan, L.-L., Liang, M.-N., Wang, D.-Q., Zhang, L.-H., Zhu, Z.-Q., and Huang, D.-L. (2019). "Dynamic adsorption of As(V) by hydroxyapatite/bagasse biomass carbon composite adsorbent," *IOP Conf. Series: Materials Science and Engineering* 490, article no. 032037. DOI:10.1088/1757-899X/490/3/032037.

Yan, Y.-B., Sarkar, B., Zhou, L., Zhang, L., Li, Q., Yang, J.-J., and Bolan, N. (2020). "Phosphorus-rich biochar produced through bean-worm skin waste pyrolysis enhances the adsorption of aqueous lead," *Environmental Pollution* 266, article no. 115177. DOI: 10.1016/j.envpol.2020.115177

Yang, W.-C., Wang, Z.-W., Song, S.-A., Han, J.-B., Chen, H., Wang, X.-M., Sun, R.-J., and Cheng, J.-Y. (2019). "Adsorption of copper(II) and lead(II) from seawater using hydrothermal biochar derived from *Enteromorpha*," *Marine Pollution Bulletin* 149, article no. 110586. DOI: /10.1016/j.marpolbul.2019.110586

Zhang, J.-J., Saho, J.-G., Jin, Q.-Z., Zhang, X., Yang, H.-P., Chen, Y.-Q., Zhang, S.-H., and Chen, H.-P. (2020). "Effect of deashing on activation process and lead adsorption capacities of sludge-based biochar," *Science of The Total Environment* 716, article no. 137016. DOI: 10.1016/j.scitotenv.2020.137016

Zhang, S., Li, X., and Chen, J. P. (2010). "An XPS study for mechanisms of arsenate adsorption onto a magnetite-doped activated carbon fiber," *Journal of Colloid and*

Interface Science 343(1), 232-238. DOI: 10.1016/j.jcis.2009.11.001

Zhang, Y., Cao, B., Zhao, L.-L., Sun, L.-L., Gao, Y., Li, J.-J., and Yang, F. (2018). "Biochar-supported reduced graphene oxide composite for adsorption and coadsorption of atrazine and lead ions," *Applied Surface Science*, 427: 147-155. DOI: 10.1016/j.apsusc.2017.07.237

Article submitted: July 2, 2021; Peer review completed: October 4, 2021; Revised version received: December 21, 2021; Accepted: December 22, 2021; Published: January 5, 2022.
DOI: 10.15376/biores.17.1.1205-1231

APPENDIX

Supplementary

Preparation of HAP-BC and BC

Bagasse was washed with water and dried in an oven at 80 °C. Dried bagasse samples were sieved by the 0.84 mm mesh sieve, collected, and stored in a desiccator.

The 250 mL of 0.2 mol L^{-1} $Ca(CH_3COO)_2$ and 250 mL of 4.4 mol L^{-1} CH_3COONH_4 were mixed into the 2000 mL beaker. A total of 50 g dried bagasse was added to the beaker and evenly mixed until the suspension was formed. The suspension was stirred for 10 min, ultrasonically shaken for 30 min, and incubated at 25 °C for 24 h. The 500 mL of 0.06 mol L^{-1} $NH_4H_2PO_4$ was added under rapid stirring, followed by slow addition of 10% (V/V) $NH_3 \cdot H_2O$ to adjust the pH to 7.5 and continued stirring for 30 min at 25 °C. The beaker was covered with a watch glass and placed in a constant temperature water bath for reaction to reach equilibrium for 48 h at 100 °C. The suspension was filtered to collect the solid precipitate. The solid precipitate was washed by ultrapure water and ethanol and dried in an oven at 70 °C for 16 h. Finally, the HAP-BC was carbonized in a muffle furnace at 500 °C for 4 h. The HAP-BC was sieved to 0.5 ~ 1 mm size fraction.

To prepare bagasse biochar, dried sugar bagasse was carbonized in a muffle furnace at 500 °C for 4 h in the absence of air. The bagasse biochar was sieved to 0.5 to 1 mm size fraction.

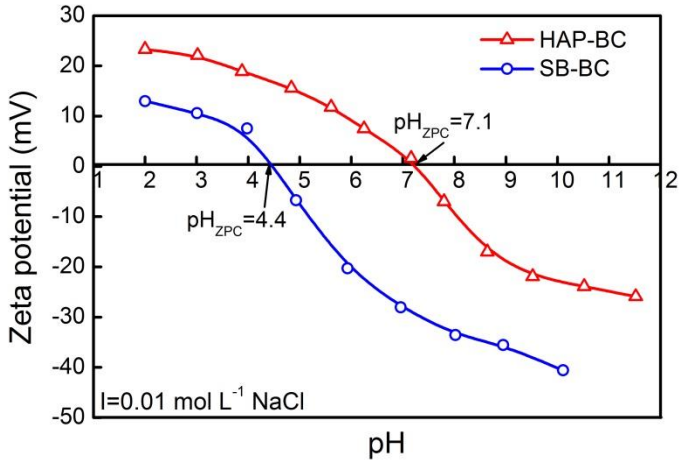

Fig. S1. Zeta potential of HAP-BC as function of pH in 0.01 mol L^{-1} NaCl electrolyte solution

Adsorption Isotherm-Freundlich isotherm

The data were fit using Freundlich adsorption models according to Eq. S1,

$$\ln q_e = \ln K_F + (\frac{1}{n}) \ln C_e \quad \text{(S1)}$$

where, q_e is the amount of Pb(II) absorbed (mg g^{-1}) at equilibrium state; C_e is the equilibrium concentration of Pb(II) in solution (mg L^{-1}); K_F (L g^{-1}) is the Freundlich

constant, which is a rough indicator of the adsorption capacity, and 1/*n* is the adsorption strength.

The values of *n* and K_F were calculated from the slope of plots and intercept (Table S1). The coefficients of determination (R^2) were found to be 0.993, 0.996, and 0.997 for the adsorption at 25, 35, and 45°C, respectively. 1/*n* is the heterogeneity factor used as a measure of the deviation from linearity of the adsorption. 1/*n* values were calculated from the slope of plots to be 0.438, 0.443, and 0.340 for the adsorption at 25, 35, and 45°C, respectively.

Table S1. Freundlich Isotherm Parameters for the Pb(II) Adsorption on HAP-BC at Different Temperature

Temperature (°C)	Freundlich		
	K_F (L g^{-1})	1/*n*	R^2
25	25.68	0.438	0.993
35	28.11	0.443	0.996
45	35.91	0.340	0.997

Adsorption Kinetics

The results of kinetic model fitting for HAP-BC adsorption of Pb(II) are shown in Fig. S2.The fitting parameters of the four models are listed in Table S2.

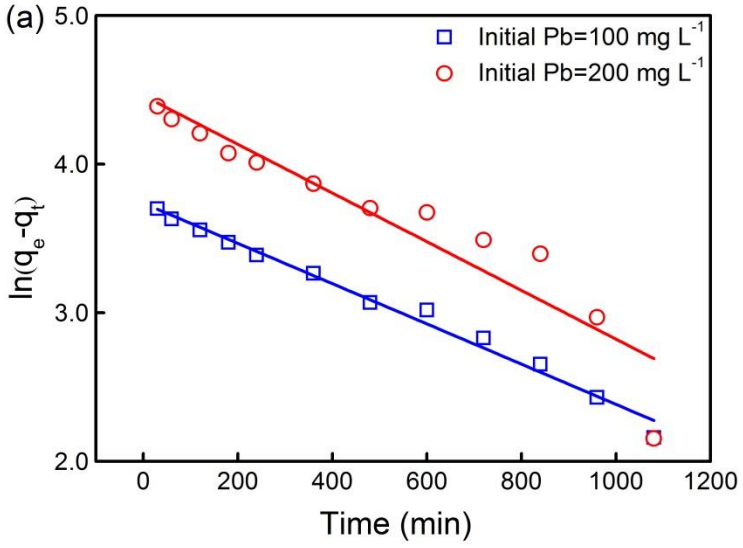

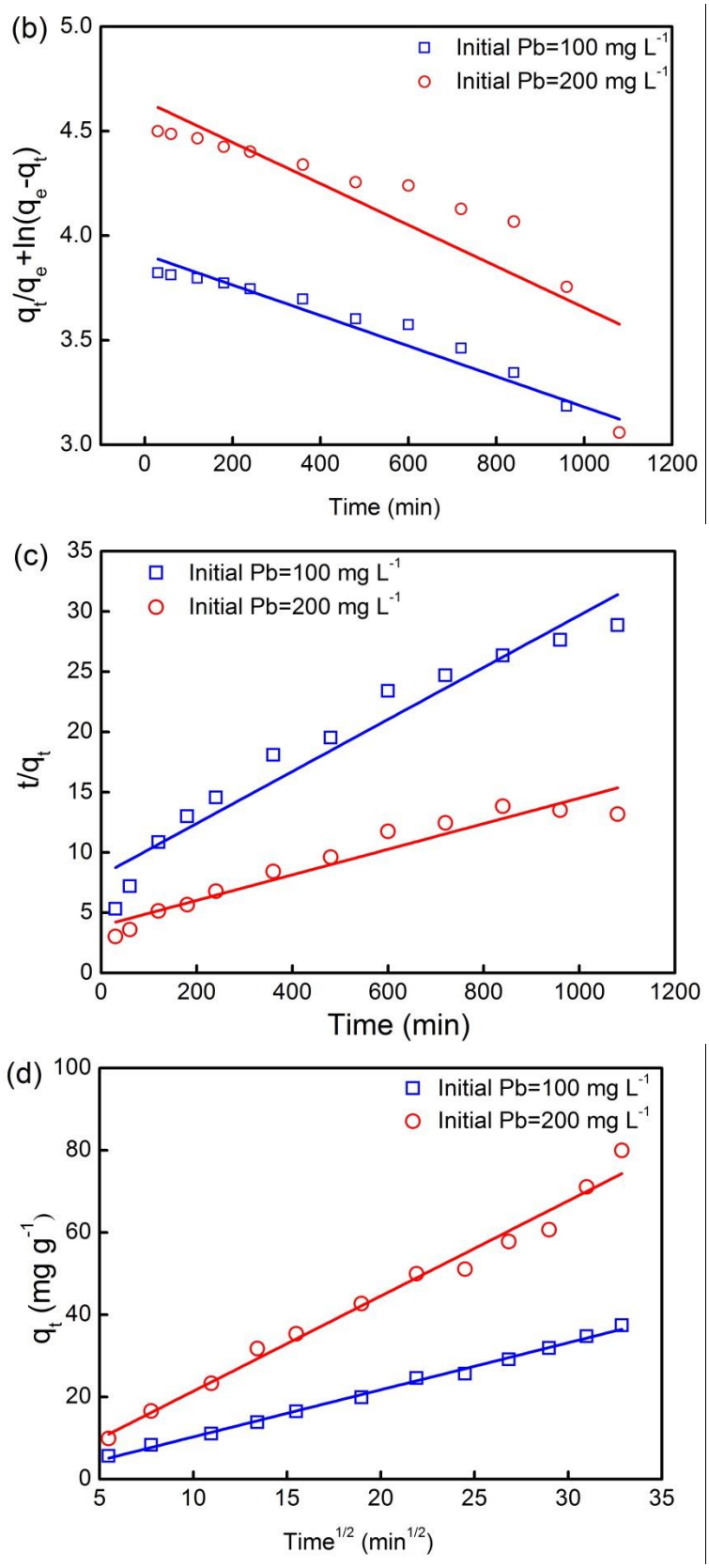

Fig. S2. Kinetics for Pb(II) adsorption onto HAP-BC(a, Pseudo-first-order kinetic model; b, Modified pseudo-first-order kinetic model; c, Pseudo-second-order kinetic model; d, Intra-particle diffusion kinetic model)

Table S2. Parameters of Kinetic for Pb(II) Sorption onto HAP-BC

Pseudo-first-order kinetic constant				
Initial Pb(II)(mg L^{-1})	K_1 (min^{-1})	q_e (mg g^{-1})	R^2	
100.0	0.0015	42.0	0.979	
200.0	0.0016	86.6	0.877	
Modified pseudo-first-order kinetic constant				
Initial Pb(II)(mg L^{-1})	K_1 (min^{-1})	q_e (mg g^{-1})	R^2	
100.0	0.00073	22.2	0.928	
200.0	0.00099	103.9	0.737	
Pseudo-second-order kinetic constant				
Initial Pb(II)(mg L^{-1})	K_2 (g $mg^{-1}min^{-1}$)	q_e (mg g^{-1})	h (g $mg^{-1}min^{-1}$)	R^2
100.0	0.417	46.5	0.110	0.939
200.0	0.011	94.3	0.256	0.954
Intra-particle diffusion kinetic constant				
Initial Pb(II)(mg L^{-1})	K_d (g $mg^{-1}min^{-1/2}$)			R^2
100.0	1.14			0.996
200.0	2.31			0.982

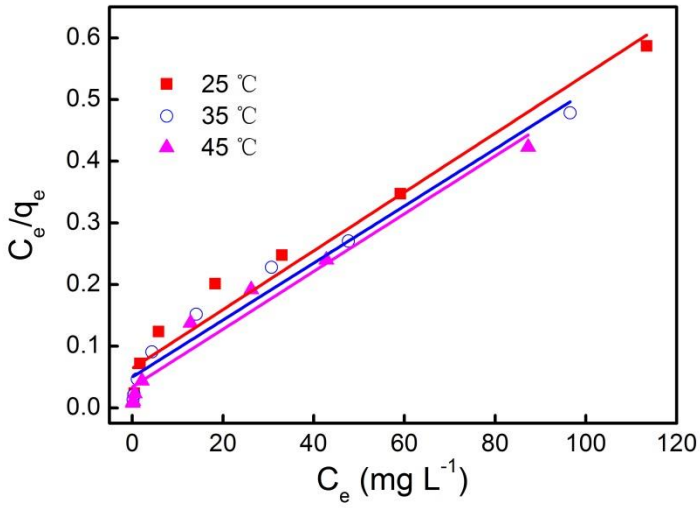

Fig. S3. Plot of linearized Langmuir adsorption isotherm

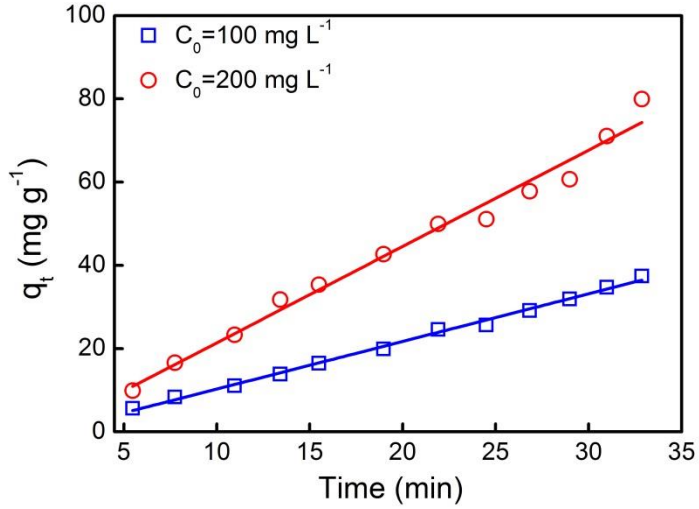

Fig. S4. Kinetics for Pb(II) adsorption onto HAP-BC intra-particle diffusion kinetic model

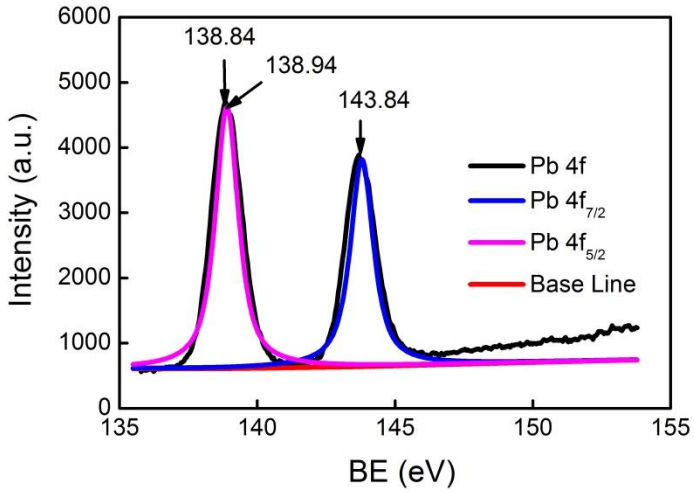

Fig. S5. Sub-peak fitted spectra of Pb4f of HAP-BC after Pb(II) adsorption

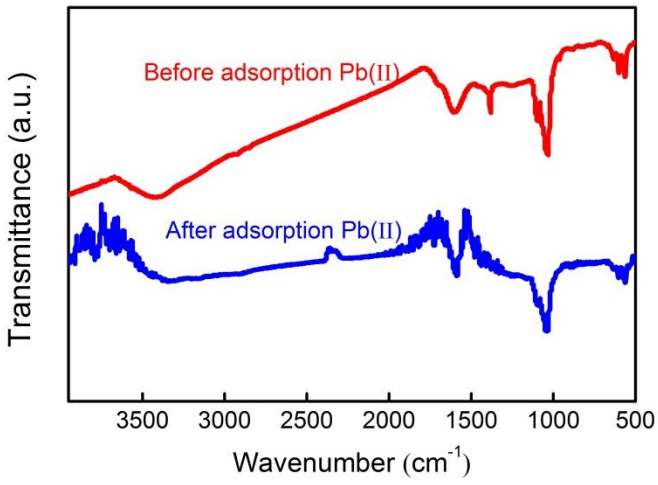

Fig. S6. FT-IR spectrogram of the HAP-BC before and after Pb(II) adsorption

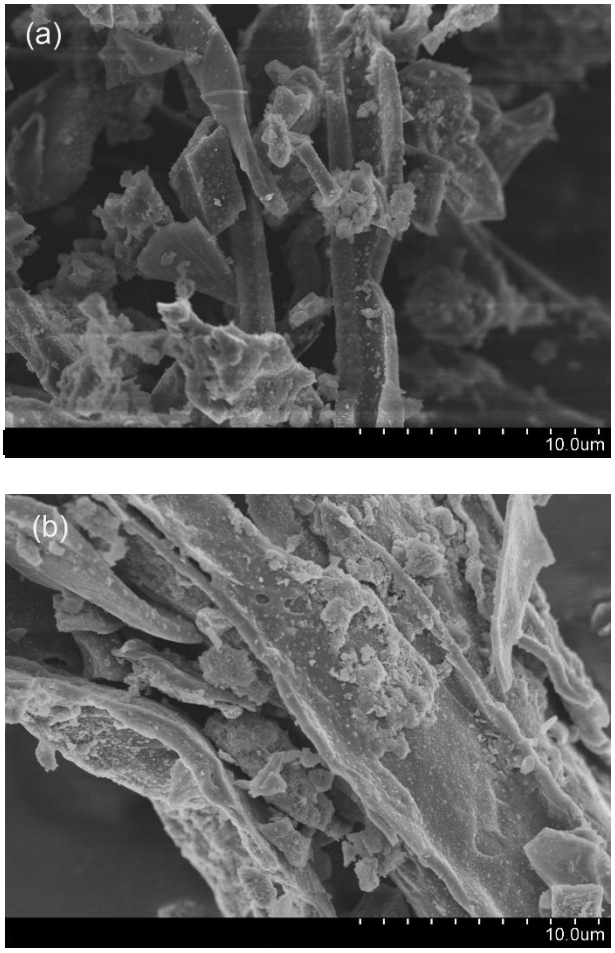

Fig. S7. SEM micrograph of HAP-BC before and after Pb(II) adsorption (a, HAP-BC; b, HAP-BC after Pb(II) adsorption)

Table S3. Mass (%) and Atomic (%) Surface Amounts on the HAP-BC Before and After Pb(II) Adsorption

Before adsorption Pb(II)			After adsorption Pb(II)		
Element	Mass(%)	Atom(%)	Element	Mass(%)	Atom(%)
C	33.45	30.53	C	25.46	23.99
O	52.48	63.79	O	54.90	68.90
P	5.08	2.39	P	4.91	2.39
Ca	8.86	3.23	Ca	11.88	4.47
Pb	/	/	Pb	2.74	0.20

Table S4. BET of HAP-BC Before and After Pb(II) Adsorption

HAP-BC	BET (m^2 g^{-1})
Before adsorption Pb(II)	89.52
After adsorption Pb(II)	83.19

Table S5. Effect of the pH on Hydroxylapatite (HAP) Ion Concentrations

pH	Calcium Concentration (mmol·L^{-1})		Phosphate Concentration (mmol·L^{-1})		Calcium to Phosphorus Molar Ratio	
	$C_{0(Pb)}$ (mg·L^{-1})		$C_{0(Pb)}$ (mg·L^{-1})		$C_{0(Pb)}$ (mg·L^{-1})	
	100	400	100	400	100	400
2.1	4.28	5.68	2.46	2.16	1.74	2.63
3.1	1.012	2.596	0.309	0.225	3.27	11.51
4.0	0.411	1.466	0.049	0.047	8.38	31.16
5.1	0.267	0.832	0.033	0.028	8.13	29.33
6.1	0.382	1.272	0.025	0.015	15.20	82.23
6.8	0.317	1.036	0.011	0.013	28.94	80.36
7.9	0.199	0.525	0.004	0.008	51.48	62.62
9.3	0.105	0.244	0.003	0.005	40.74	47.30